Supplementary Information

Chain-configuration and rate dependent rheological properties in transient networks

M. K. Sing, Z. Wang, G. H. McKinley, and B. D. Olsen

System parameters and steady-state convergence criteria

For purposes of this work, a mesh size of $\Delta\tilde{x} = \Delta\tilde{y} = \Delta\tilde{z} = 0.25$ was used. Steady state equilibrium was determined using the less stringent of the two error criteria as defined below:

$$\text{Absolute Error} = \frac{abs\left(\psi_{dangling,\tilde{t}} - \psi_{dangling,\tilde{t}-1}\right)}{\Delta\tilde{t}} = 1x10^{-12} \quad \backslash^* \text{ MERGEFORMAT (1)}$$

$$\text{Relative Error} = \frac{abs\left(\psi_{dangling,\tilde{t}} - \psi_{dangling,\tilde{t}-1}\right)}{\psi_{dangling,\tilde{t}-1}\Delta\tilde{t}} = 1x10^{-5} \quad \backslash^* \text{ MERGEFORMAT (2)}$$

The time step used was determined using the maximum value of the FENE force relative to the spatial discretization and rounded for convenience.

$$\Delta\tilde{t} = 0.1^*10^{floor\left[\log\left[\frac{\Delta\tilde{x}}{\max\left(\tilde{F}_{FENE}\right)}\right]\right]} \quad \backslash^* \text{ MERGEFORMAT (3)}$$

Equation and numerical method validation

The equations used are derived from the *Smoluchowski* equation for convection and diffusion. In order to validate the numerical methodology and results used in this work, the results for a dangling chain in steady and oscillatory shear flow were compared to the results of the upper-convected Maxwell Model solved for the aforementioned cases. The spring potential was changed from a finitely extensible (FENE) spring to a Hookean spring.

$$\underline{\underline{\sigma}} + \tau \overset{\nabla}{\underline{\underline{\sigma}}} = \eta_o \underline{\underline{\dot{\gamma}}} \qquad \text{* MERGEFORMAT (4)}$$

In small shear, the normal stresses σ_{11} and σ_{22} are zero and the upper-convected Maxwell Model * MERGEFORMAT (4) reduces to:

$$\left(1 + \tau \frac{\partial}{\partial t}\right)\sigma_{12} = \eta_o \dot{\gamma}_{12} \qquad \text{* MERGEFORMAT (5)}$$

In oscillatory shear, equation * MERGEFORMAT (5) becomes:

$$\left(1 + \tau \frac{\partial}{\partial t}\right)\sigma_{12} = \eta_o \gamma_o \omega \cos(\omega t) \qquad \text{* MERGEFORMAT (6)}$$

Equations * MERGEFORMAT (5) and * MERGEFORMAT (6) can be non-dimensionalized using the variables below:

$$\tilde{\sigma} = \frac{\sigma}{\upsilon k_B T} \qquad \text{* MERGEFORMAT (7)}$$

$$\tilde{\omega}' = \omega \tau_R \qquad \text{* MERGEFORMAT (8)}$$

$$\tilde{t}' = \frac{t}{\tau_R} = \frac{tH}{\zeta} \qquad \text{* MERGEFORMAT (9)}$$

$$\tilde{G} = \frac{G}{\upsilon k_B T} \ . \qquad \text{* MERGEFORMAT (10)}$$

Given that the zero shear-rate viscosity can be expressed as:

$$\eta_o = G \tau_R \ , \qquad \text{* MERGEFORMAT (11)}$$

equations * MERGEFORMAT (5) and * MERGEFORMAT (6) become:

$$\frac{\partial \tilde{\sigma}_{12}}{\partial \tilde{t}'} + \tilde{\sigma}_{12} = \tilde{\sigma}_{o,12} \qquad \text{* MERGEFORMAT (12)}$$

and

$$\frac{\partial \tilde{\sigma}_{12}}{\partial \tilde{t}'} + \tilde{\sigma}_{12} = \tilde{G}\tilde{\omega}'\gamma_o \cos\left(\tilde{\omega}'\tilde{t}\right), \qquad \text{* MERGEFORMAT (13)}$$

respectively. Equations * MERGEFORMAT (12) and * MERGEFORMAT (13) can then be solved in the case of small shear as linear first order differential equations to get the solutions for equation * MERGEFORMAT (4) in start-up steady shear and oscillatory shear flow. These equations are then compared to the solutions for the dimensionless *Smoluchowski* equation:

$$\frac{d\psi}{d\tilde{t}} = (1/3)\tilde{\nabla}_r^2\psi + \tilde{\nabla}_r \bullet \left(\psi \tilde{F}_{Hookean}\right) - De \bullet \tilde{r}_y \tilde{\nabla}_r \psi \quad \text{* MERGEFORMAT (14)}$$

The $\tilde{t}$ used in equation * MERGEFORMAT (14) represents the fact that the chain relaxation time used to non-dimensionalize time is different from the relaxation time used in equations * MERGEFORMAT (12) and * MERGEFORMAT (13) by a factor of two such that $2\tilde{t}' = \tilde{t}$.

Comparison with start-up steady shear

For start-up of steady shear, the solution to equation * MERGEFORMAT (12) is:

$$\tilde{\sigma}_{12}\left(\tilde{t}'\right) = \tilde{\sigma}_{o,12}\left[1 - \exp\left(-\tilde{t}'\right)\right] \qquad \text{* MERGEFORMAT (15)}$$

Given that the chain relaxation times used to non-dimensionalize equations * MERGEFORMAT (14) and * MERGEFORMAT (15) differ by a factor of two, the numerical results can be compared to the Maxwell Model using a modified form of equation * MERGEFORMAT (15):

$$\tilde{\sigma}_{12}\left(\tilde{t}\right) = \tilde{\sigma}_{o,12}\left[1 - \exp\left(-2\tilde{t}\right)\right] \qquad \text{* MERGEFORMAT (16)}$$

When $\tilde{\sigma}_{12}/\tilde{\sigma}_{o,12}$ is graphed for multiple shear rates as a function of time, the resultant steady shear curves overlap.

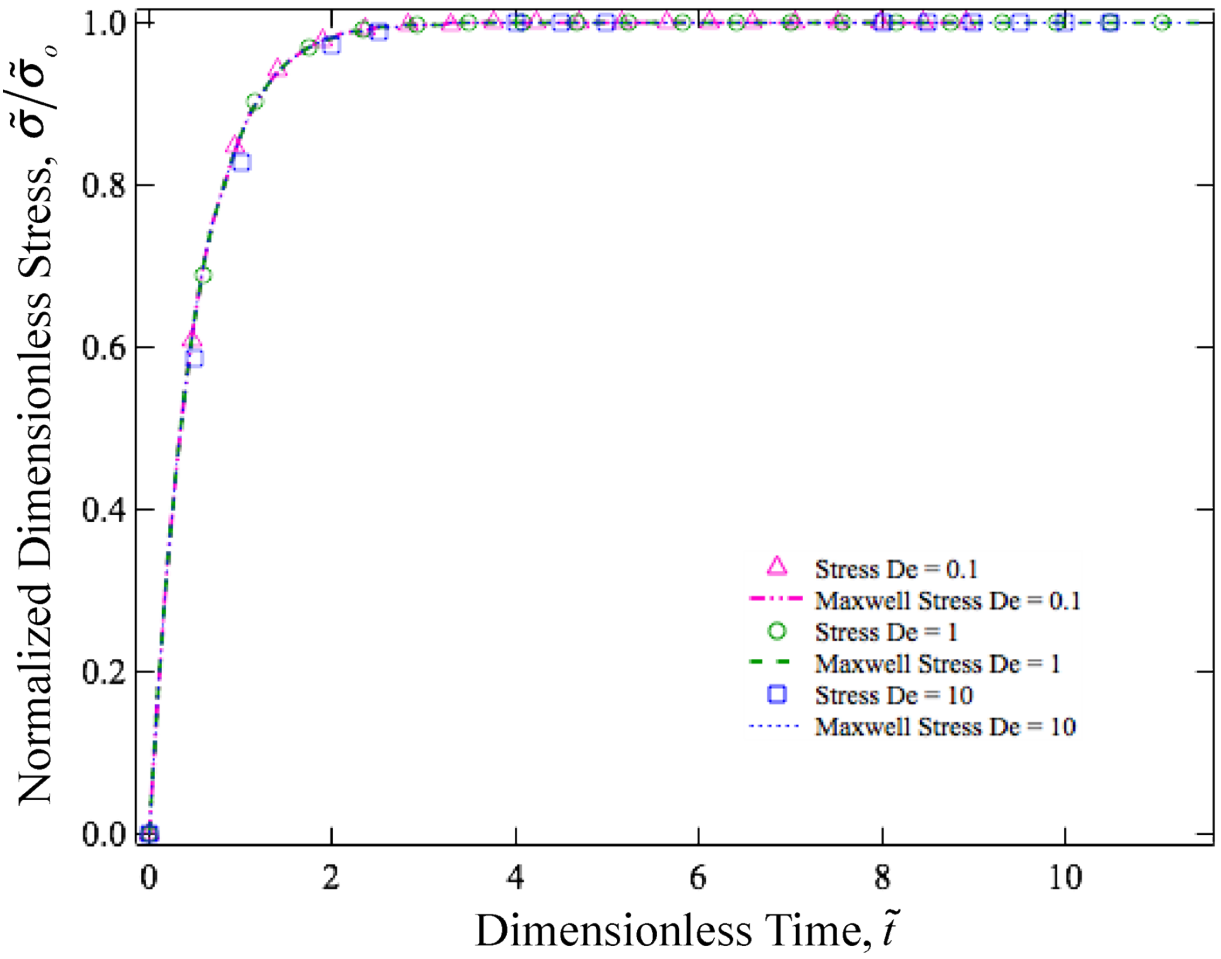

Fig. S1: Steady shear data from theoretical calculations compared with results to the upper convected Maxwell Model. Calculations used only dangling chains acted on by a Hookean Spring.

Comparison with small amplitude oscillatory shear (SAOS)

For oscillatory shear, the solution to equation * MERGEFORMAT (13) is:

$$\tilde{\sigma}_{12}\left(\tilde{t}'\right)=\tilde{G}\gamma_o\left\{\frac{\left[\left(\tilde{\omega}'\right)^2\sin\left(\tilde{\omega}'\tilde{t}'\right)+\tilde{\omega}'\cos\left(\tilde{\omega}'\tilde{t}'\right)\right]}{\left(\tilde{\omega}'\right)^2+1}\right\} \quad \text{* MERGEFORMAT (17)}$$

This resultant equation is best rewritten in terms of the in-phase and out-of-phase portions of the modulus:

$$G' = \frac{\tilde{G}(\tilde{\omega}')^2}{(\tilde{\omega}')^2 + 1} \qquad \text{* MERGEFORMAT (18)}$$

$$G'' = \frac{\tilde{G}\tilde{\omega}'}{(\tilde{\omega}')^2 + 1}\ , \qquad \text{* MERGEFORMAT (19)}$$

where G' represents the storage modulus (in-phase) and G" represents the loss modulus (out-of-phase). When an oscillatory shear rate ($De = \gamma_o \tilde{\omega} \cos(\tilde{\omega}\tilde{t})$) is used in equation * MERGEFORMAT (14), the corresponding stress response is analyzed relative to the imposed shear rate, and the correct relative angular frequencies ($\tilde{\omega}' = \tilde{\omega}/2$) are used, the resultant storage and loss moduli for the Maxwell model and the numerically calculated theoretical model overlap.

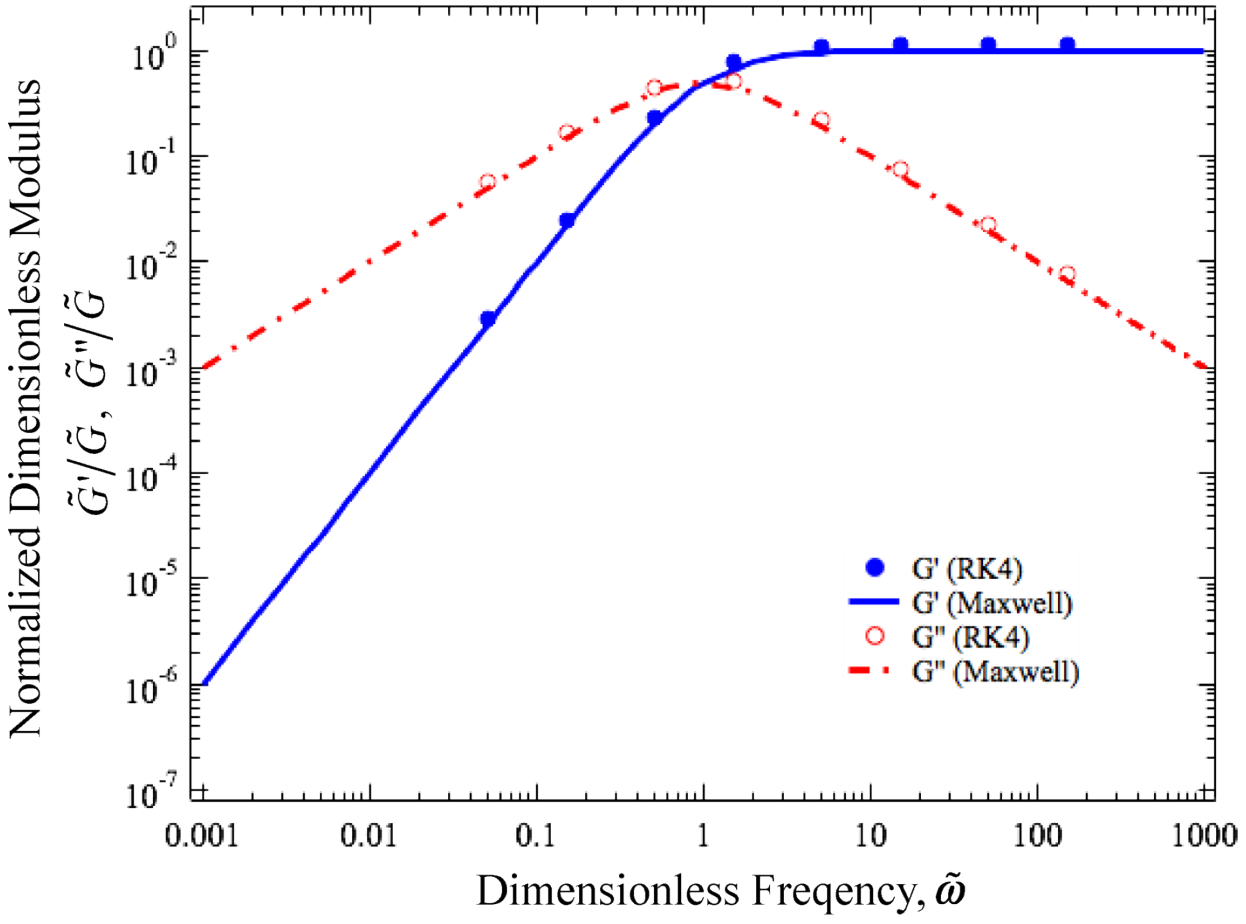

Fig. S2: SAOS data for theoretical calculations compared to results of Maxwell Model solved for oscillatory shear. Calculations used only dangling chains acted on by a Hookean Spring.

Comparison with experiment and simulation

A variety of shear and extensional experiments have been performed on single chain molecules. Larson, et al. compared DNA in steady shear with multiple chain models, including FENE bead-spring models.[1] When the shear data from for overall extension in Larson's paper is compared with the shear data for root mean square end-to-end distance from the theory that is the focus of this work, there is reasonable agreement. It should be noted that there is a discrepancy due to the simulation's ability to calculate the chain extension found experimentally whereas this work can only predict the value of $\langle \tilde{x}^2 \rangle^{1/2}$, resulting in lower values relative to the FENE spring simulation. While direct comparison is difficult, the resultant values for the numerical solutions to the theory used in this work provide reasonable agreement with previously published works.

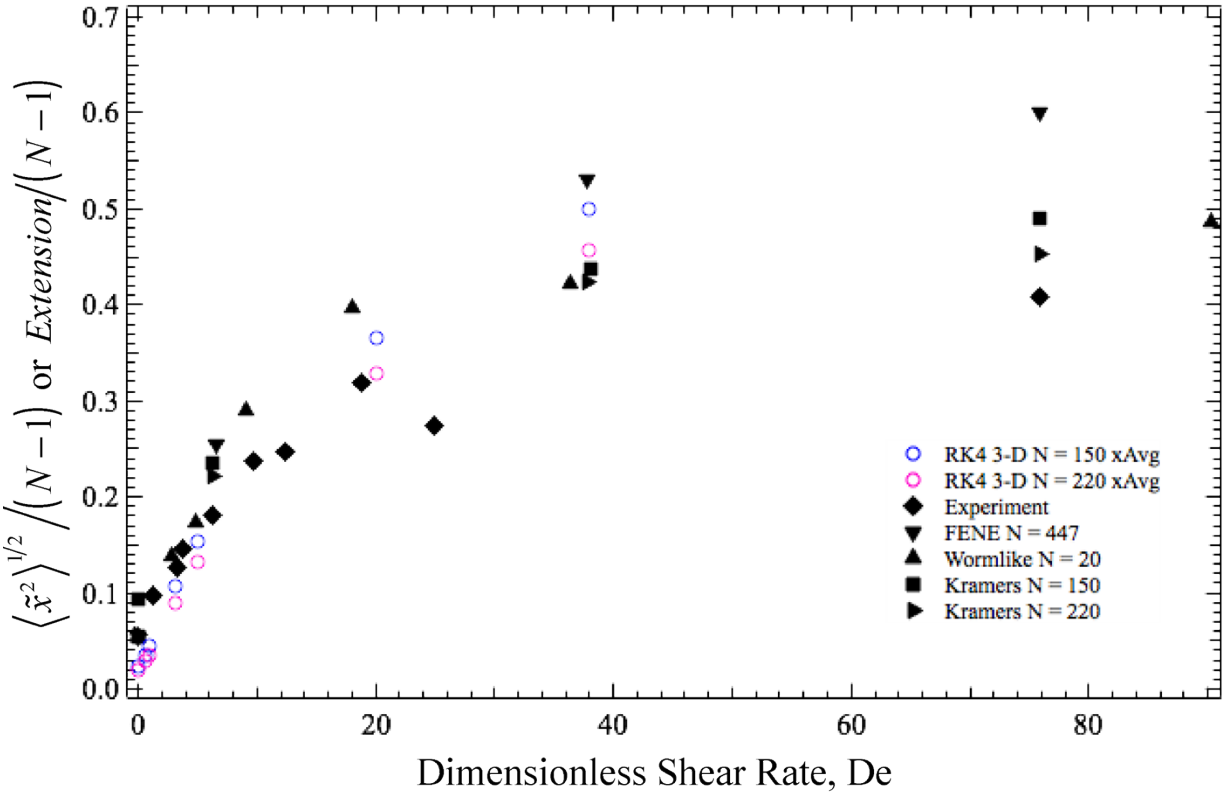

Fig. S3: Normalized extension in the flow-vorticity plane for simulations of a FENE chain, a wormlike chain, a Kramers chain, and DNA compared to normalized root-mean-square end-to-end distance in the flow-vorticity plane for two values of N from this work (empty circles).

Validation of kinetic terms

In order to validate the reaction kinetics, all systems used in this work were solved without shear until equilibrium was reached. When the final equations for dangling, bridged, and looped chains are solved assuming equilibrium conditions ($d\psi/d\tilde{t}=0$), the equilibrium constant K_{eq} for the rates of dissociation verses association can be solved for between both dangling and looped chains and dangling and bridged chains (respectively):

$$K_{eq,\,Dangling\leftrightarrow Looped}=\frac{\int\left[f(\tilde{r})\psi_{Dangling}\right]d\tilde{r}}{\psi_{Looped}} \quad \backslash^* \text{ MERGEFORMAT (20)}$$

$$K_{eq,\,Dangling\leftrightarrow Bridged}=\frac{\int\left[\left(1-f(\tilde{r})\right)\psi_{Dangling}\right]d\tilde{r}}{\int\left[\psi_{Bridged}\exp\left(\beta\left|\tilde{F}_{FENE}\right|\right)\right]d\tilde{r}} \quad \backslash^* \text{ MERGEFORMAT (21)}$$

Using the equilibrium probability distributions, the actual K_{eq} can be calculated using equations * MERGEFORMAT (20) and * MERGEFORMAT (21) and compared with the imposed value of K_{eq}, to match within 1% error. The particular kinetic terms used in this work fall within physical ranges for associating gels.[2, 3]

System mesh size

For purposes of this work, all results were obtained using a mesh size of $\Delta\tilde{x}=\Delta\tilde{y}=\Delta\tilde{z}=0.25$. The expected $\left\langle\tilde{r}^2\right\rangle^{1/2}$ for a Gaussian chain is 1. In all of the systems studied, $\left\langle\tilde{r}^2\right\rangle^{1/2}$ at De = 0 was approximately 1.09 due to finite discretization of the mesh. For comparison, a mesh size of $\Delta\tilde{x}=\Delta\tilde{y}=\Delta\tilde{z}=0.1$ was used resulting in equilibrium $\left\langle\tilde{r}^2\right\rangle^{1/2}$ of 1.037; however, the calculation time increased to impractical lengths. For the systems discussed in the main text, the values for $\left\langle\tilde{r}^2\right\rangle^{1/2}$ at equilibrium are shown in Table S1.

k_a	K_{eq}	$\langle r^2 \rangle_D^{1/2}$	$\langle r^2 \rangle_B^{1/2}$
2	0.01	1.09	1.09
2	0.05	1.09	1.09
2	0.2	1.09	1.09
0.7	0.01	1.09	1.09
0.7	0.05	1.09	1.09
0.7	0.2	1.09	1.09
0.2	0.01	1.09	1.10
0.2	0.05	1.09	1.09
0.2	0.2	1.09	1.09

Table S1: Equilibrium root mean square end-to-end distance values for systems shown in Fig. 6.

Determination of Dangling Chain Flux

In order to investigate tethered chain tumbling, the flux of the system was determined from the non-dimensionalized form of the *Smoluchowski* equation:

$$\frac{\partial \psi_i}{\partial \tilde{t}} = (1/3)\tilde{\nabla}_r^2 \psi_i + \tilde{\nabla}_r \bullet \left(\psi_i \tilde{F}_{FENE}\right) - De \bullet \tilde{r}_y \tilde{\nabla}_r \psi_i + R_i \quad \backslash^* \text{ MERGEFORMAT (22)}$$

where 'R' represents the reaction terms for chain interconversion and 'i' designates the chain conformation. Given the definition of flux:

$$\frac{\partial \psi}{\partial \tilde{t}} + \tilde{\nabla} \bullet \tilde{j} = R, \qquad \backslash^* \text{ MERGEFORMAT (23)}$$

The dimensionless flux corresponds to the sum of the convective, diffusive, and retractive components of equation * MERGEFORMAT (22) when the divergence is factored out:

$$\tilde{j} = -(1/3)\tilde{\nabla}\psi_i - \psi_i \tilde{F}_{FENE} + \left(De \bullet r_y\right)\psi_i \qquad \backslash^* \text{ MERGEFORMAT (24)}$$

Detailed stress results

The phase map obtained in the main document was created by graphing dimensionless stress as a function of dimensionless strain rate for all systems studied. Monotonic stress curves exhibit continuously increasing stress with increasing shear rate. Systems where the stress decreases at any point with increasing shear rate are considered to be undergoing some form of instability.

The figures below show dimensionless stress as a function of dimensionless shear rate for different dimensionless association rates as a function of different equilibrium constants.

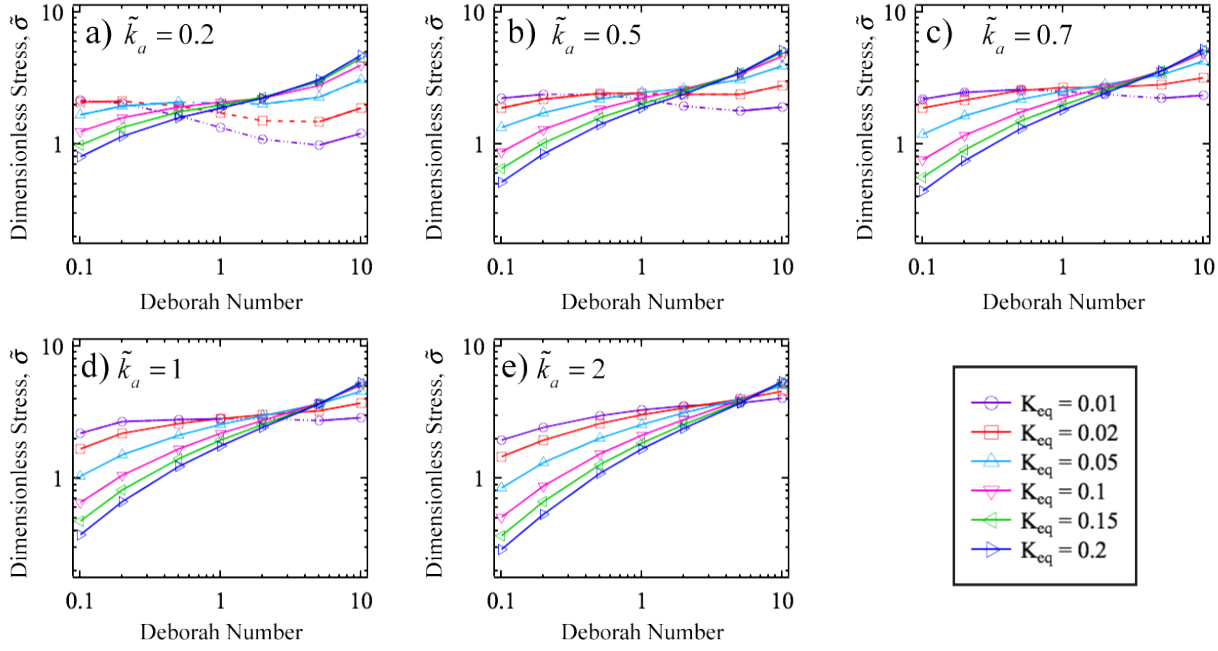

Fig. S4: Stress in steady shear for all systems tested, graphed in groups according to imposed values of dimensionless association rate ($\tilde{k}_a$) for different values of K_{eq}. Dotted lines in a, b, c, and d indicate non-monotonic stress behaviour. For all graphs, K_{eq} decreases from bottom to top at low shear rates and increases for De = 10.

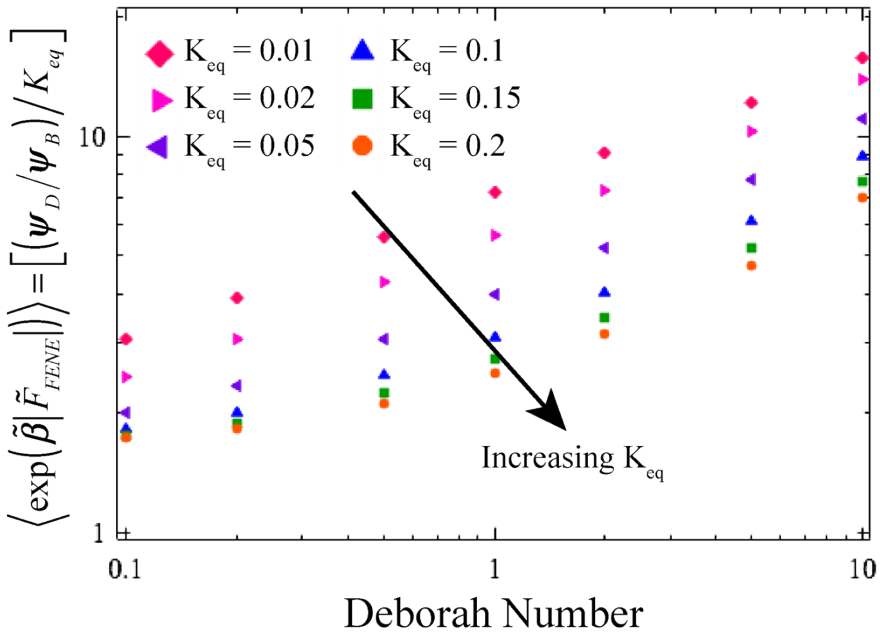

Fig. S5: Average of Bell's Law exponential term for $\tilde{k}_a = 0.7$ (middle row of Fig. 5 and 7), where a value of $\left\langle \exp\left(\tilde{\beta}\left|\tilde{F}_{FENE}\right|\right)\right\rangle$ greater than 2 corresponds to $\left\langle \tilde{r}^2 \right\rangle_B^{1/2}$ increasing at a slower rate (curve is concave down) with increasing De. The spatial average of the Bell's Law term increases with decreasing K_{eq}. The increased magnitude corresponds to the increased chain end extension when dissociation is less favored at low K_{eq}.

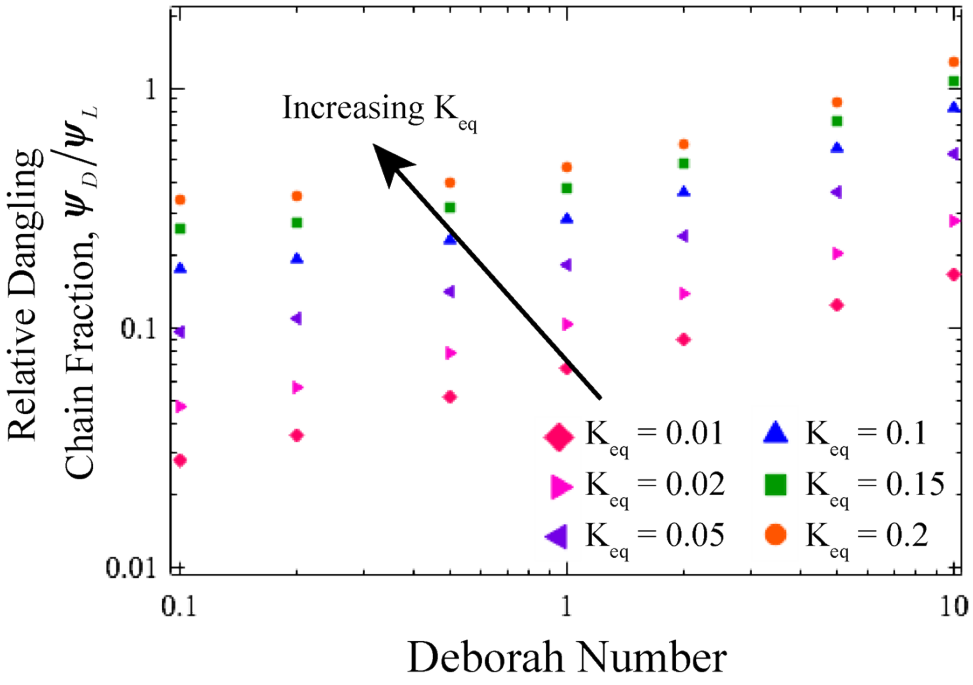

Fig. S6: Relative dangling chain fraction compared to looped chain fraction for $\tilde{k}_a = 0.7$. In all systems, the ratio between dangling and looped chain fractions increases with increasing shear rate despite the non-monotonic behavior in looped chain fractions.

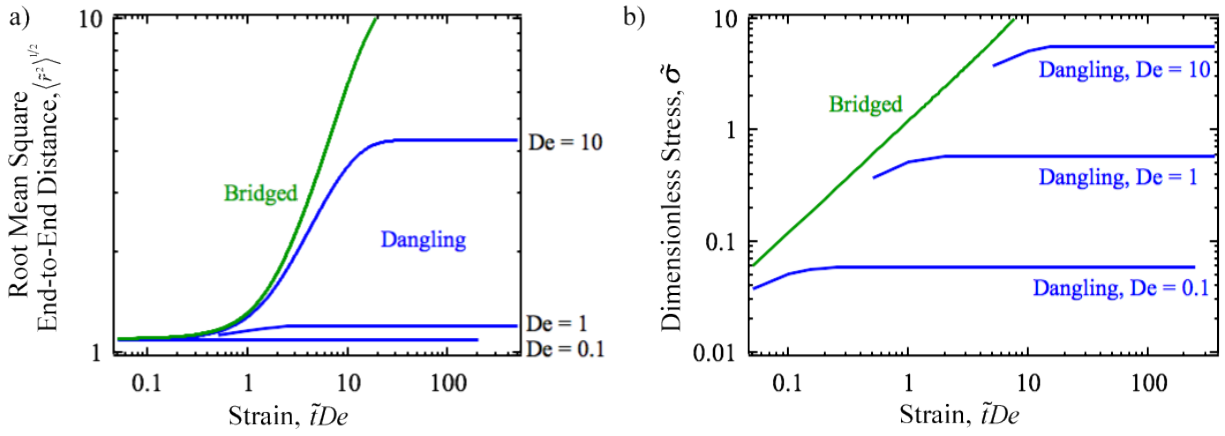

Fig. S7: Start-up (a) extensional and (b) stress behaviour of bridged (green dashed line) and dangling chains (blue multi-length dashed line) in shear (no reaction terms) for different shear rates. In the case of bridged chains, all shear rates overlap.

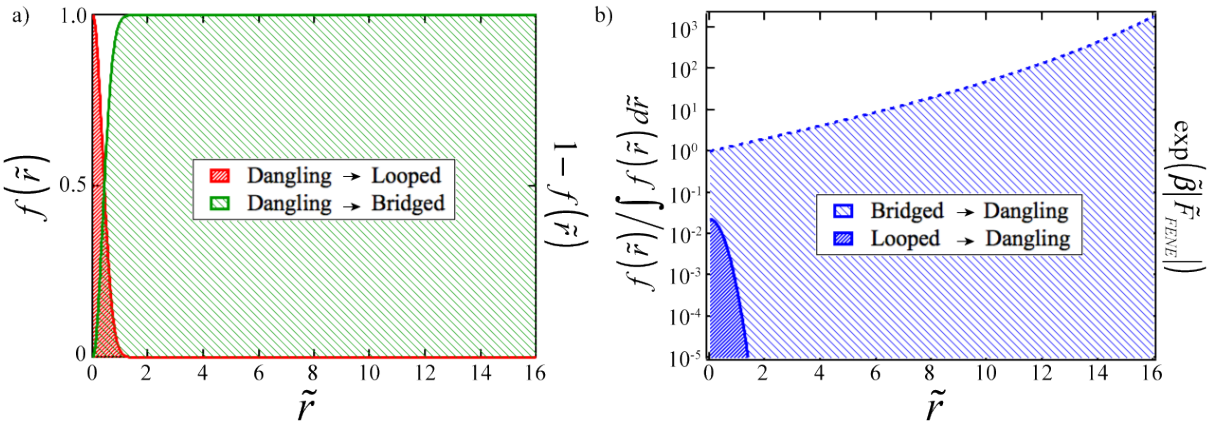

Fig. S8: Schematic representation of (a) Gaussian probabilities for dangling chain association to either a looped or bridged chain and (b) looped or bridged dissociation to form a dangling chain as a function of radial position. The y-axis in (b) is on a log-scale and looped chains are assumed to only exist at the origin (no extension) such that the dark blue region represents the probability of a loop forming a dangling chain with an extension $\tilde{r}$.

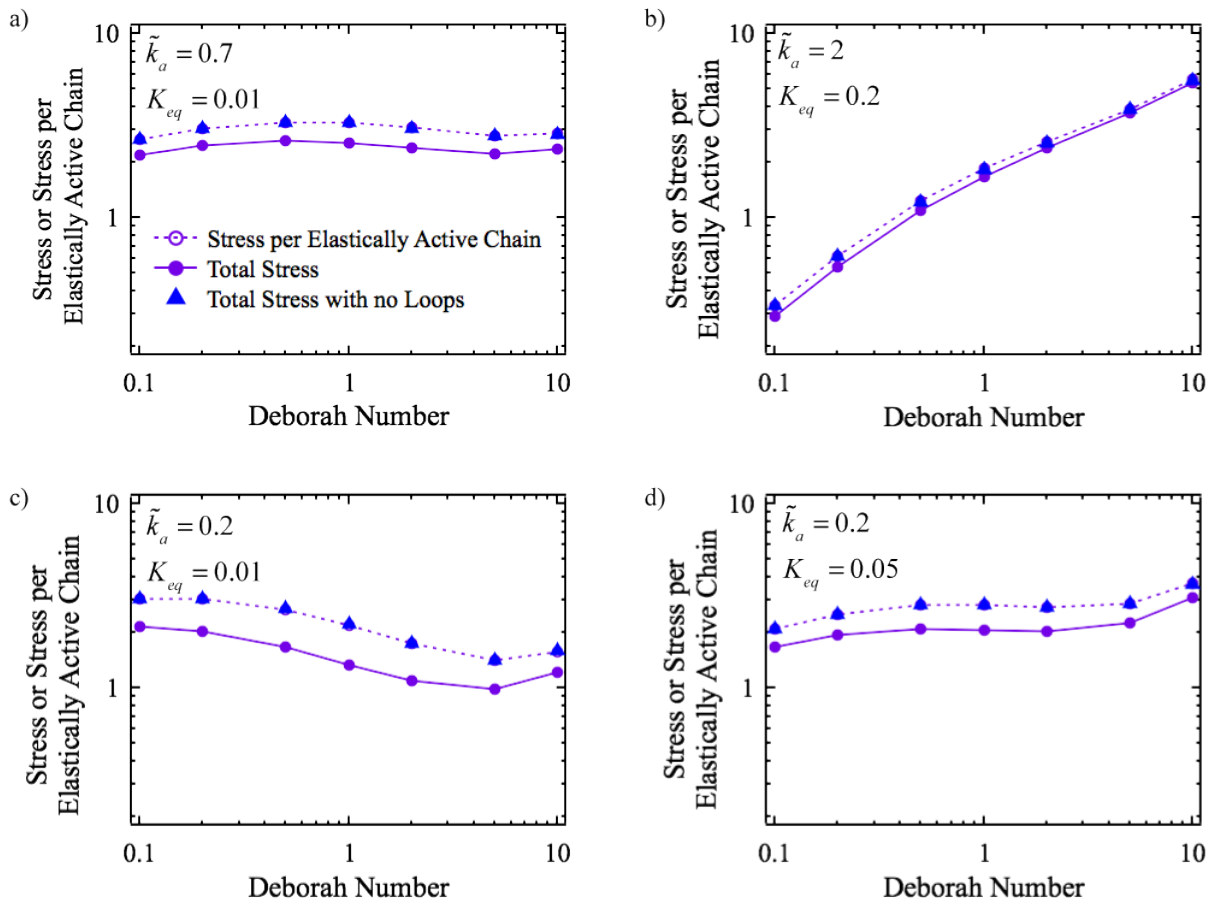

Figure S9: Comparison between systems with the probability of forming looped chains and systems that only contain dangling and bridged chains. In all four cases shown here, the total stress without looped chains corresponds to the stress per elastically effective chain when loop formation is allowed. Therefore, presence of loops results in a decrease in total stress and earlier onset of stress instabilities without changing average chain extension. Since the total stress is normalized by $\upsilon k_B T$ where υ corresponds to the number density of polymer chains and the fraction of elastically active chains is dimensionless, the dimensions on the total stress, the total stress with no loops, and the stress per elastically active chain are equivalent.

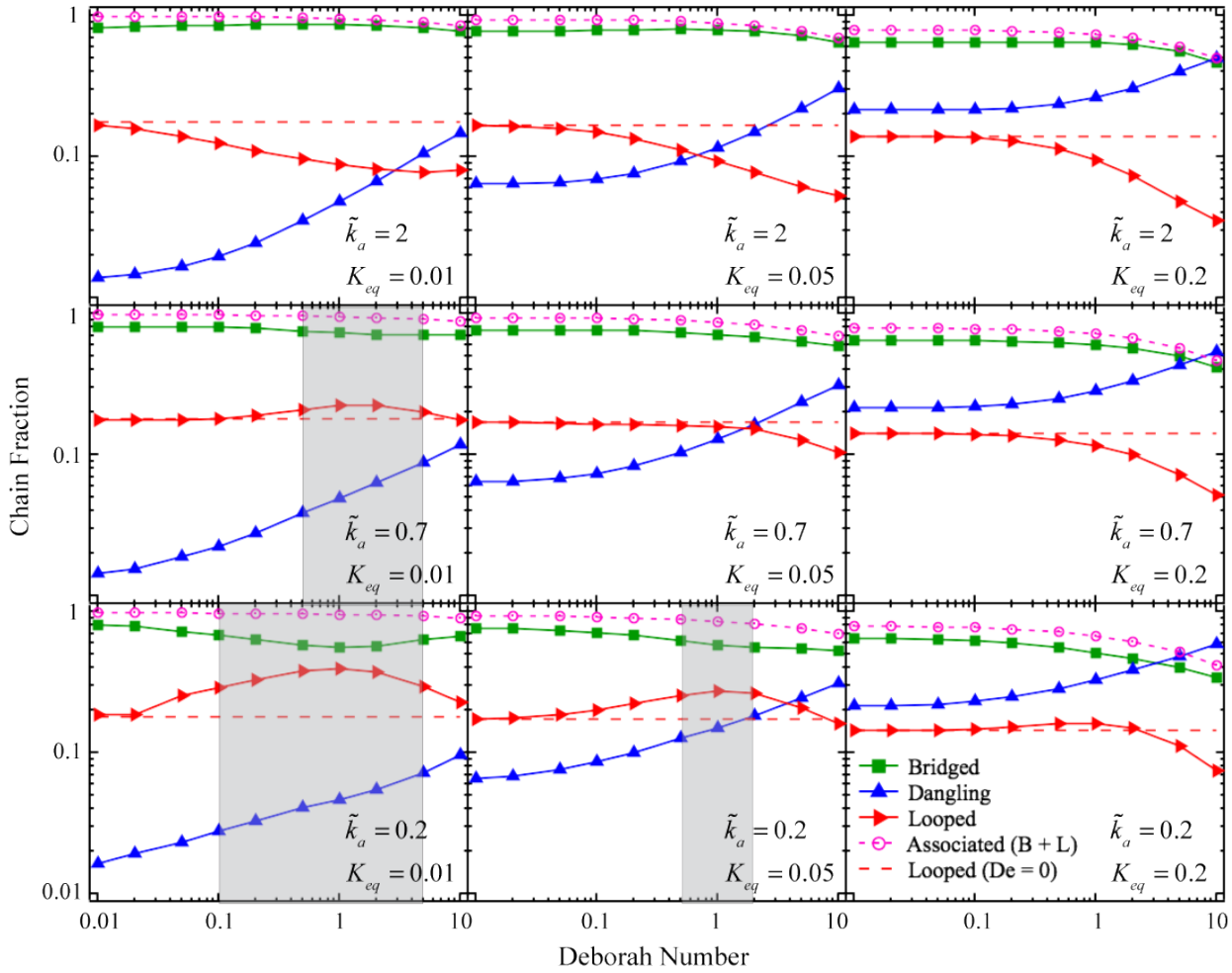

Fig. S10: Chain fraction behavior as a function of De, $\tilde{k}_a$, and K_{eq}. Equilibrium values increase from left to right, while the dimensionless association rate decreases from top to bottom. Shaded areas correspond to regions of unstable stress.

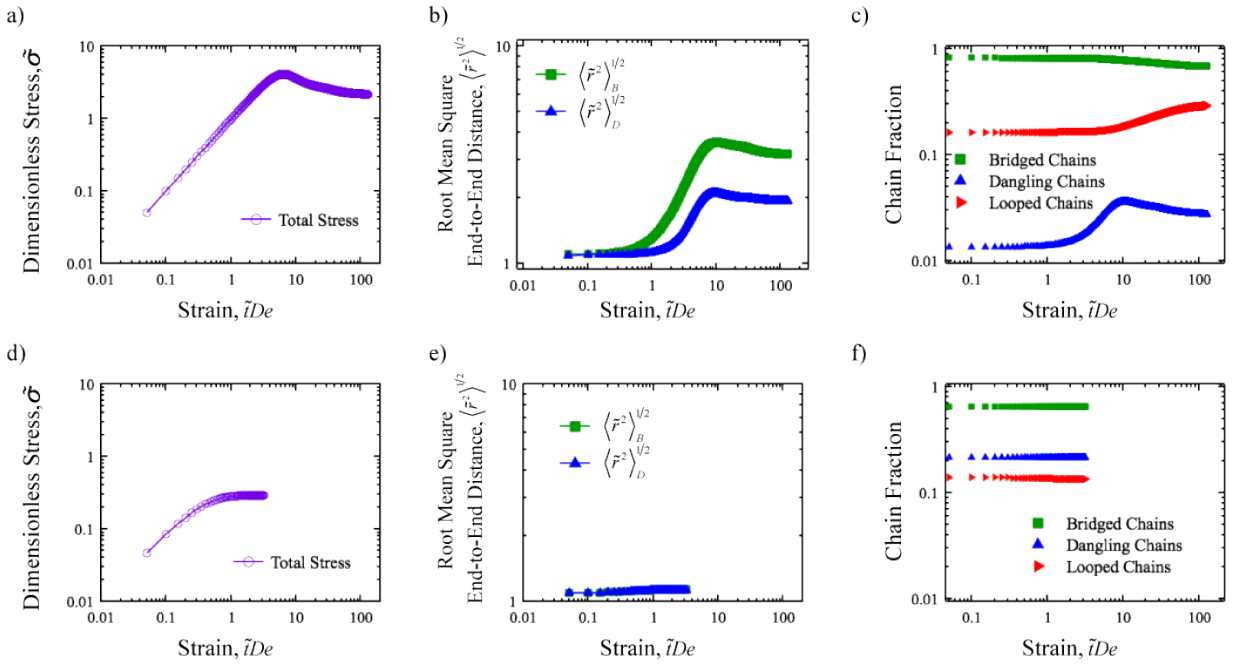

Fig. S11: Transient chain fraction data for $\tilde{k}_a = 0.2$, $K_{eq} = 0.01$ (a - c) and $\tilde{k}_a = 2$, $K_{eq} = 0.2$ (d - f) at De = 0.1 demonstrating representative behavior for systems with monotonic and non-monotonic stress in steady state.

References

1. J. S. Hur, E. S. G. Shaqfeh and R. G. Larson, *J Rheol*, 2000, **44**, 713-742.
2. L. Zhang, E. M. Furst and K. L. Kiick, *J Control Release*, 2006, **114**, 130-142.
3. W. C. Yount, D. M. Loveless and S. L. Craig, *Angew Chem Int Edit*, 2005, **44**, 2746-2748.